Magnetometer bias insensitive magnetic field matching based on pedestrian dead reckoning for smartphone indoor positioning

Jian Kuang, Taiyu Li, Xiaoji Niu

***Abstract*— Magnetic field signals are ubiquitous, stable, and have little effect on the human body. Due to these qualities magnetic field matching (MFM) has become a popular indoor positioning method and has attracted considerable attention within the smartphone geolocation community. However, the need to frequently calibrate the magnetometer bias seriously undermines the applicability and stability of MFM. In this paper we present a magnetometer bias insensitive MFM based on pedestrian dead reckoning (PDR) for smartphones in the indoor environment. An inertial navigation system based PDR is designed for generating the relative trajectory and attitude. The relative trajectory is used to correlate the magnetic field feature time sequence to improve the distinguishability and the attitude is used for projecting the reference magnetic field feature from n-frame to b-frame, to perform the MFM in the b-frame to eliminate the influence of the magnetometer bias. The results of eight experiments in four smartphones showed that the proposed method could effectively eliminate the influence of the magnetometer's bias in the MFM, and finally reached mean positioning accuracy of 0.77 m (RMS).**

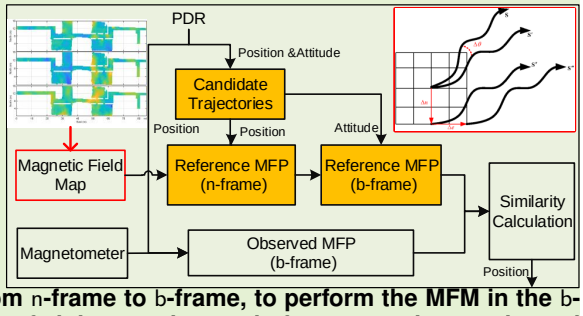

***Index Terms*— INS, PDR, MM, indoor positioning, magnetic matching, pedestrian navigation**

I. Introduction

LOCATION based service (LBS) is gradually changing people's lifestyles and work styles through services such as positioning and navigation, social networking, precise advertising, and emergency rescue [1]. As global navigation satellite systems (GNSSs) are hindered by signal attenuation and blockage in certain environments (e.g., indoor and subterranean environments), a number of indoor positioning technologies have been developed for providing ubiquitous location services, such as pseudo-satellites [2], ZigBee [3], ultra-wideband (UWB) [4], audio positioning [5], radio frequency identification (RFID) [6], WiFi [7], magnetic field matching (MFM) [8]and pedestrian dead reckoning (PDR) [9].

Due to the huge difference in cost and accuracy, it is challenging for a positioning technology fulfill the requirements of specific scenarios with complex and diverse indoor structural environment [10]. For consumer applications, the successful requirements of which are low-cost and wide-area coverage, the positioning technology is severely limited. As magnetic field signals are ubiquitous, stable, and have little effect on the human body, the magnetic field feature based method has become one of the mainstream indoor positioning methods [8].

This work was supported by the National Key Research and Development Program of China (2016YFB0502202 and 2016YFB0501803). (Corresponding author: Xiaoji Niu.)

J. Kuang, X. Niu and T. Li are with the GNSS Research Center, Wuhan University, Wuhan, Hubei 430072 China (E-mails:kuang@whu.edu.cn; taiyuli@whu.edu.cn; xjniu@whu.edu.cn).

MFM is not commonly used as a standalone technique for similar magnetic field features (MFFs) can be found in many different places. To alleviate this issue, MFM is integrated with other techniques such as PDR and wireless localization [11]. Many MFM methods have been used to provide positioning services. Particle filter (PF) based MFM methods [12] have a simple deign where the filter individually processes a magnetometer measurement while the PDR is used to propagate the state of particles and recursively re-samples a set of particles according to the comparison between the measured and the reference MFFs to converge on the true position. The best performance can be obtained by setting thousands of particles. However, heavy calculation of PF is still a problem that needs to be solved urgently for smartphones.

Dynamic time warping (DTW) based methods [13] provide a precise position for users by revisiting the historical trajectory stored in the magnetic field map during the positioning phase. Because an effective constraint cannot be formed for the user's walking trajectory in an open area, the positioning performance of these methods are usually unstable. An alternative is to combine the grid magnetic field map and the PDR algorithm to adapt to the impact of different indoor scenes by real-time estimation of user trajectory [8]. DTW is currently the most widely used MFM method due to its low calculation and stable positioning performance.

Although MFM can provide a high-precision position, the magnetometer built in smartphones is vulnerable to ferromagnetic material (e.g., the magnets inside audio speakers and

buzzers) or strong electric currents, which often result in a magnetic distortion known as soft and hard iron effects [14]–[16]. These magnetic influences of soft magnetic effects can be reduced through careful circuitry design [14]. Hard iron distortion causes an equivalent bias in magnetometer measurements that needs to be accurately calibrated and compensated [15]. Several methods have been proposed for compensating the bias of magnetometers in the literature. The conventional "∞" motion-based magnetometer bias calibration requires user to calibrate it for dozens of seconds or more [17], and other calibration techniques that require extra knowledge of the magnetic field at the location of interest are not available in standard indoor environments [16].

Many researchers have employed the differential MFF (DMFF) to reduce the influence of the magnetometer bias. [18] assumes that the projection of the magnetometer bias in the vertical direction can be regarded as a fixed value; therefore, the DMFF in the vertical direction is independent to the magnetometer bias. Similarly, [10] uses the horizontal, vertical, and amplitude of the DMFF. [19] uses the variance of the MFF between two consecutive steps instead of using the MFF to avoid the magnetometer bias. The above methods can only achieve the expected performance when the fluctuation of the smartphone attitude is small. However, it is almost impossible for the user to hold the smartphone in a fixed posture and only walk on a straight track; thus, the change in the attitude of the smartphone will prevent the DMFF in the n-frame from eliminating the magnetometer bias.

In this study, we assume that the magnetometer's bias has not changed over short time periods (e.g., 15 s), and that the misalignment angle between the mobile phone's orientation and the user's walking direction is small. A strapdown inertial navigation system (INS) based PDR is designed to generate the relative trajectory of a user and the attitude (i.e., absolute roll, pitch and relative heading) of the smartphone. The relative trajectory is used to correlate the MFF to improve the distinguishability and reduce the search area by predicting the current position in the positioning phase. The attitude coming from PDR and the absolute heading search algorithm in the MFM are used for obtaining the conversion relationship from the navigation frame (n-frame) to the sensor frame (b-frame), to perform the MFM in the b-frame for eliminating the influence of the magnetometer bias. In addition, the output of MFM is employed to control the position error of PDR, which will further improve the positioning performance by estimating the scale of the user's step length. Finally, four smart phones of different brands are used to verify the feasibility and positioning performance of the method in this study.

The contributions of the present paper are summarized as follows: Based on the relative trajectory and attitude of the smartphone generated by PDR, a magnetic field matching algorithm without magnetometer bias correction is designed. The algorithm uses the PDR algorithm to estimate the attitude of the mobile phone in real-time, and no longer assumes that the change of the attitude of the mobile phone is small, so as to truly realize the magnetic field matching algorithm independent of the magnetometer bias.

The remainder of the paper is organized as follows: Section II analyzes the feasibility of using the differential magnetic field feature in the b-frame to eliminate the magnetometer bias, Section III describes the indoor positioning solution process; Section IVgives a detailed description of the INS-based PDR algorithm, including INS mechanization, the designed EKF, and pedestrian motion constraint; Section V shows a detailed description of the magnetic field matching algorithm; Section VI investigates the positioning performance of the proposed method through field tests; Section VII discusses the proposed method; and Section VIII details our conclusions.

II. Differential Magnetic Field Feature

Based on the simplified model of the magnetometer measurements, the relationship between magnetometer observations and the reference MFF in the n-frame can be described as

$$M^n = C_b^n M^b = C_b^n \left(\tilde{M}^b - b_m \right) \tag{1}$$

where M^b represents the reference magnetic field feature in the b-frame, while $\tilde{M}^b$ and b_m represent the measurements and bias of the magnetometer, respectively, M^n represents the reference MFF in the n-frame, C_b^n represents the direction cosine matrix from b-frame to n-frame. Given that the reference MFF at two positions M_1^n and M_2^n, and the difference between the two can be described as

$$M_2^n - M_1^n = C_{b,2}^n \tilde{M}_2^b - C_{b,1}^n \tilde{M}_1^b + \left(C_{b,1}^n - C_{b,2}^n \right) b_m \tag{2}$$

From Eq. 2, we know that the magnetometer bias can be eliminated when $C_{b,1}^n$ and $C_{b,2}^n$ are approximately equal, such as the user holds the smartphone steadily and walks in a straight trajectory. However, it is unrealistic for the user to keep the attitude of the smartphone fixed and only walk in a straight line. Fig. 1 shows the horizontal, vertical, and amplitude of the DMFF (at 10 Hz) obtained with a smartphone (Google Pixel2) in the real environment, where the red and blue lines represent the calibrated and un-calibrated DMFF in the n-frame, respectively. Due to the existence of a large magnetometer bias (approximately 600 milligauss), the weak fluctuation of the horizontal angle still causes the vertical component of the DMFF to fluctuate sharply (as shown in Fig. 1-(b)). Additionally, the change of the heading angle formed by the turning motion of the user directly destroys the waveform shape of the horizontal and amplitude (as shown in Fig. 1-(a) and (c)).

The magnetometer bias is a fixed vector in the b-frame for a period of time (e.g., 15 s); therefore, we change the Eq. 1 to derive

$$\tilde{M}^b = (C_b^n)^T M^n + b_m \tag{3}$$

Then, the DMFF between the two given positions in the b-frame can be described as

$$\tilde{M}_2^b - \tilde{M}_1^b = (C_{b,2}^n)^T M_2^n - (C_{b,1}^n)^T M_1^n \tag{4}$$

Eq. 4 shows that the DMFF in b-frame will no longer be related to the magnetometer bias. Thus, the most critical issue is how to accurately obtain C_b^n and its corresponding geographic position. The following chapters of this article will describe in detail how to use the relative trajectory and attitude provided

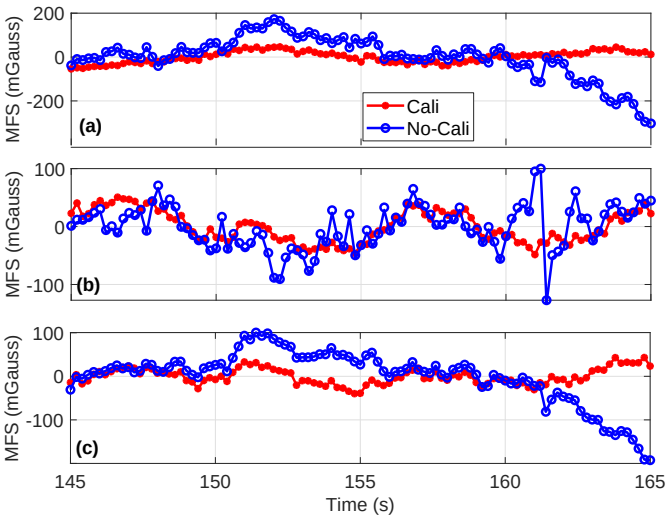

Fig. 1. The horizontal, vertical and amplitude of the DMFF. (a) Horizontal, (b) Vertical, (c) Amplitude.

by PDR to implement the MFM algorithm that is independent of the magnetometer bias.

III. System Overview

The efficacy of magnetic field matching is limited by two factors: 1) the indoor MFF has a low discriminability when in position; 2) the magnetometer bias suffers relatively extreme drift and requires frequent calibration. The relative trajectory provided by PDR can be used to improve the discriminability of MFF and reduce the search area of the MFM algorithm by predicting the current position while the attitude provided by PDR is able to obtain the conversion relationship between the navigation (n-frame) and sensor (b-frame) frames to eliminate the effects of magnetometer bias. In addition, the results of MFM are used to correct the position error of the PDR and estimate the error of the sensor and the step length. Thus, with low system construction cost, MFM/PDR considerably improve the usability of the system by using complementary characteristics of the two, which may help solve the problem of indoor positioning of consumers in the future.

Fig. 2 shows the detailed process of INS-based PDR based magnetic field matching for smartphone indoor positioning. The system can be divided into two parts: the INS based PDR method and magnetic matching algorithm. Gyroscope and accelerometer measurements are used to perform INS mechanization and determine the user's motion states (i.e., static or walking), and the virtual velocity measurements from the user's motion are employed for controlling the velocity error, which assist in improving the estimation accuracy of the relative trajectory and attitude.

Based on the relative trajectory estimated by INS-based PDR, many candidate trajectories are generated by adjusting the translation and rotation parameters. The corresponding reference magnetic field profile (MFP) in the n-frame can be obtained by querying in the magnetic field map. The attitude is used to convert the reference MFP from n-frame to b-frame. Currently, the observed MFP is generated by correlating the relative trajectory coming from the INS-based PDR and the magnetometer observations. Thus, the current position of the user can be determined by calculating similarities between the differential observed and reference magnetic profiles.

To obtain a more accurate relative trajectory and predicted current position, the MFM output will be used to control the position error of the INS-based PDR and estimate errors in the sensors and step length.

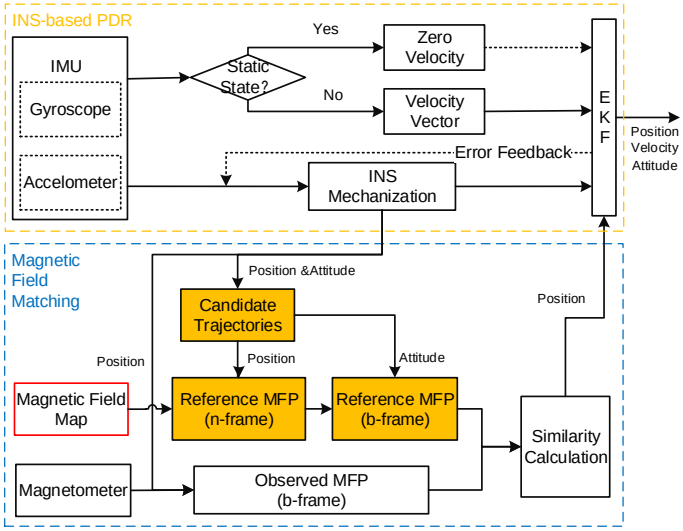

Fig. 2. The detailed process of INS-based PDR based magnetic field matching for smartphone indoor positioning.

IV. INS-based Pedestrian Dead Reckoning

The relative trajectory coming from the PDR method are necessary to improve the distinguishability of the MFF. As the step-model based PDR method separates the position error from the sensors error, estimating the sensors error cannot be achieved by correcting the position error. Additionally, the output frequency is low (e.g., 2 Hz), which cannot reflect the actual movement of the user. This study use an INS-based PDR method to generate relative trajectory for improving positioning performance of the magnetic field matching method.

A. INS Mechanization

The INS mechanization mainly provides current position, velocity, and attitude by continuously integrating the gyroscope and accelerometer output, using an algorithm with a long development history and a rigorous theoretical structure. Due to the low performance of smartphone sensors, the complex error corrections in the rigorous INS mechanization (e.g., earth rotation) cannot bring about improvements in navigation performance. Therefore, the simplified INS mechanization is given by [9], [20], [21]

$$\begin{cases} r_k^n = r_{k-1}^n + v_k^n \Delta t_k \\ v_k^n = v_{k-1}^n + C_{b,k}^n \left(\Delta v_k^b\right) - g^n \Delta t_k \\ C_{b,k}^n = C_{b,k-1}^n \left[I + \Delta\theta_k^b \times\right] \end{cases} \tag{5}$$

where r^n and v^n are the position vector and the velocity vector in the n-frame, respectively, C_b^n is the transformation matrix

from the b-frame to the n-frame, $g^n = \begin{bmatrix} 0 & 0 & -g \end{bmatrix}^T$ is the Earth gravity vector, $\Delta v_k^b = \left(\tilde{f}_k^b - b_{f,k} \right) \Delta t_k$ is the velocity increment in the b-frame, $\tilde{f}^b$ and b_f are the acceleration and bias of the accelerometer, respectively. $\Delta \theta_k^b = \left(\tilde{\omega}_k^b - b_{g,k} \right) \Delta t_k$ is the angle increment in the b-frame, $\tilde{\omega}^b$ and b_g are the angle rate and bias of the gyroscope, respectively. $\Delta t = t_k - t_{k-1}$ is the time interval between the $(k-1)$-th and k-th epoch, and "$\times$ " is the cross-product form of a vector.

B. Extended Kalman Filter

The position error of the INS mechanization algorithm grows quadratically with time, and the navigation performance depends substantially on the sensor accuracy. For smartphone built-in inertial sensors, the estimated position of the INS mechanization method will develop an error of more than 10 m in a few seconds, well beyond acceptable parameters for real world application. However, pedestrian motion characteristics can be used to construct virtual observations, thereby slowing down the cumulative speed of the position errors. An extended Kalman filter is used to fuse the constraint information coming from pedestrian motion and INS. The 16-dimensional error state variables are defined as

$$\delta x = \begin{bmatrix} \delta r^n & \delta v^n & \phi & \delta b_g & \delta b_a & \delta s \end{bmatrix}^T \tag{6}$$

where δr^n, δv^n are the position and velocity error vector in the n-frame, and ϕ is the attitude error vector. δb_g, δb_a are the bias error vectors of the gyroscope and accelerometer, δs is the scale error of step length. Because the empirical model cannot adapt to different users, the step scale factor is used as an estimation variable for improving the accuracy of the step-length estimation.

The discrete linearization of the system error model can be expressed as follows:

$$\begin{cases} \delta x_{k,k-1} = \Phi_{k,k-1} \delta x_{k-1,k-1} + w_k \\ \delta z_k = H_k \delta x_{k,k-1} + v_k \end{cases} \tag{7}$$

where the subscripts $k-1$ and k represent the epoch, δz is the measurement misclosure vector, H is the design matrix, w is the process noise, v is the measurement noise, and Φ is the 16 × 16 state transition matrix

$$\Phi_{k,k-1} = \begin{bmatrix} I_3 & I_3 \Delta t & 0_3 & 0_3 & 0_3 & 0_{3\times 1} \\ 0_3 & I_3 & (f_k^n \times) \Delta t & 0_3 & C_{b,k}^n \Delta t & 0_{3\times 1} \\ 0_3 & 0_3 & I_3 & -C_{b,k}^n \Delta t & 0_3 & 0_{3\times 1} \\ 0_3 & 0_3 & 0_3 & I_3 & 0_3 & 0_{3\times 1} \\ 0_3 & 0_3 & 0_3 & 0_3 & I_3 & 0_{3\times 1} \\ 0_{1\times 3} & 0_{1\times 3} & 0_{1\times 3} & 0_{1\times 3} & 0_{1\times 3} & 1 \end{bmatrix} \tag{8}$$

where 0_3 and I_3 are 3×3 zero matrix and identity matrix, $0_{1\times 3}$ and $0_{3\times 1}$ are 1×3 and 3×1 zero matrix. When the observations are valid, the following methods are used to update the state variables and corresponding covariance [20].

$$\delta \hat{x}_k = \delta \hat{x}_{k,k-1} + K_k \left(\delta z_k - H_k \hat{x}_{k,k-1} \right) \tag{9}$$

$$P_k = \left(I - K_k H_k \right) P_{k,k-1} \left(I - K_k H_k \right)^{\mathrm{T}} + K_k R_k K_k^T \tag{10}$$

$$K_k = P_{k,k-1} H_k^T \left(H_k P_{k,k-1} H_k^T + R_k \right)^{-1} \tag{11}$$

C. Pedestrian Motion Constraint

User movement can be divided into two states: standing still and forward motion. There are multiple ways to use the output of tri-gyroscopes and tri-accelerators to distinguish the state of the user [9]. When the state of the pedestrian is determined to be standing, the velocity can be reasonably considered to be zero. A velocity observation equation in the n-frame for zero velocity is given by:

$$\delta z_v = \hat{v}_{ins}^n - \begin{bmatrix} 0 & 0 & 0 \end{bmatrix}^T = \delta v^n + n_v \tag{12}$$

where $\hat{v}_{ins}^n$ is the velocity vector coming from the INS mechanization in the n-frame and n_v is the measurement noise. In addition, the assumption of constant heading is also commonly used to reduce the accumulation error of the heading. However, weak motion from the user's arm will destroy the above assumption; therefore, the constant heading is not considered for ensuring the stability of the system in this study.

When the user walks forward regularly, the lateral and vertical velocities in the body coordinate system should be zero [9], because a pedestrian generally walks on a plane and rarely walk sideways or backwards. The walking velocity can be estimated by step detection and step length. The peak detection algorithm is employed to detect a step event for its lower computation, and the Weinberg model is utilized to estimate the step length due to less-estimated parameters [22]. Thus, the virtual velocity measurement in the b-frame are expressed as follows:

$$\begin{aligned} \tilde{v}_{walking}^b =& \begin{bmatrix} (s+\delta s) L/\Delta t & 0 & 0 \end{bmatrix}^T + n_v \\ =& v_{walking}^b + \begin{bmatrix} L/\Delta t & 0 & 0 \end{bmatrix}^T \delta s + n_v \end{aligned} \tag{13}$$

where $v_{walking}^b = \begin{bmatrix} sL/\Delta t & 0 & 0 \end{bmatrix}^T$ represent the velocity measurement in the b-frame, L is the estimated step length from the Weinberg model, s and δs are the scale and scale error of step length, and Δt is the time interval between two adjacent steps. The predicted velocity from INS mechanization in b-frame can be expressed as

$$\hat{v}_{ins}^b = \hat{C}_n^b \hat{v}_{ins}^n \approx v_{ins}^b + C_n^b \delta v^n - C_n^b \left(v^n \times \right) \phi \tag{14}$$

where v_{ins}^n is the velocity vector in the n-frame coming from the INS mechanization, $v_{ins}^b = C_n^b v_{ins}^n$ is the velocity in the b-frame and the velocity observation equation in the b-frame is given by [9], [20], [23]

$$\begin{aligned} \delta z_v =& \hat{v}^b - \tilde{v}^b \\ =& C_n^b \delta v^n - C_n^b \left(v^n \times \right) \psi - \begin{bmatrix} L/\Delta t & 0 & 0 \end{bmatrix}^T \delta s + n_v \end{aligned} \tag{15}$$

V. Magnetic Field Matching Algorithm

The MFM positioning scheme mainly consists of two phases: magnetic field map generation and online positioning. In the magnetic field map generation phase, a one-to-one correspondence between the geographic coordinates and the MFF is established. In the online positioning phase, the current position of the user is determined by calculating the similarities between the measured MFF and the reference MFF from the magnetic field map (i.e., magnetic field matching algorithm).

As this study focuses on the MFM algorithm, no detailed description of the magnetic field map generation are provided; the similar method can be found in [8]. And the difference is that this paper uses a pedestrian positioning and orientating system (P-POS) to provide the coordinates of the data collection trajectory and the attitude of the smartphone. The P-POS has low cost and simple operation, and can provide decimeter-level position and degree-level attitude estimation, the detail algorithm can be found in [25].

A. Observed Magnetic Field Profile

The MFF of one position contains at most three-dimensional components (i.e., the north, east, and vertical components), which is insufficient to distinguish different locations. Therefore, the magnetometer measurements in a period of time (i.e., the MFF time sequence) is usually used as the basic unit for the magnetic field matching algorithms. Considering the strong correlation between the MFF distribution and the spatial structure, we correlate the MFF time sequence with the relative trajectory generated by the PDR (i.e., MFP) [9]. The directional changes and distance to the adjacent MFF can be given by the magnetic profile in addition to the interval time of the adjacent MFF. An observed magnetic field profile follows:

$$oMFP = \left\{ \begin{array}{ccc} r_1^n & (C_b^n)_1 & \tilde{M}_1^b \\ & \cdots & \\ r_k^n & (C_b^n)_k & \tilde{M}_k^b \end{array} \right\} \tag{16}$$

where $r^n = [n \quad e]$ represents the north and east position, C_b^n represents the transformation matrix from the b-frame to the n-frame, $\tilde{M}^b$ represents the measurements of magnetometer, and k represents the length.

Although the relative trajectory generated by PDR also have deformation errors (such as heading drift error and the scale error of step length), the scale error of step length can be estimated by using the results of the MFM to update navigation state. For the heading drift error, the test results of a large number of documents show that the cumulative error of PDR in a short time (such as 15 s) is negligible [9]; therefore, this study does not consider the heading drift error of the magnetic profile.

B. Candidate Reference Magnetic Field Profiles

After the MFFs and the relative trajectory are correlated, the MFM algorithm can be described as finding the conversion relationship (i.e., the translation and rotation parameters) between the relative trajectory and the absolute trajectory. Because the absolute trajectory and the conversion relationship must both be solved, they cannot be solved directly by analytical mathematics. Here, we determine the conversion relationship by enumerating all possible reference trajectories. In order to control the computational load, the low precision predicted position (such as 10 m) and the radius of the search region (such as 10 m) are parameters determined in advance.

Fig. 3 demonstrates using the traversal method to generate candidate trajectories. First, we extract the relative trajectory S generated by PDR, then rotate $\Delta\theta$ around the left endpoint of S to obtain trajectory S', then translate Δn along the north-south direction to obtain trajectory S'', and finally translate Δe along the east-west direction to obtain trajectory S'''.

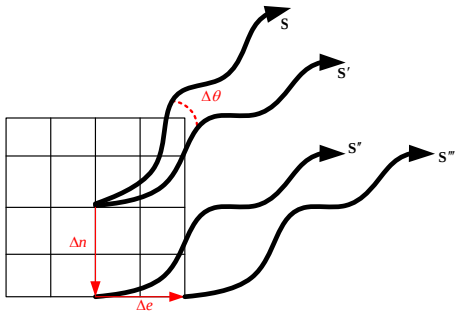

Fig. 3. The generation process of the candidate trajectories.

The trajectory S''' can be expressed as

$$r_{i,j}^{n'} = C\left(\Delta\theta_i\right)\left(r_j^n - r_1^n\right) + r_1^n + \Delta r_i^n \tag{17}$$

$$C\left(\Delta\theta_i\right) = \left[\begin{array}{cc} \cos\left(\Delta\theta_i\right) & -\sin\left(\Delta\theta_i\right) \\ \sin\left(\Delta\theta_i\right) & \cos\left(\Delta\theta_i\right) \end{array} \right] \tag{18}$$

where r_j^n are the position of the j-th point of the relative trajectory, respectively, $r_{i,j}^n$ is the position of the j-th point of the i-th candidate trajectory, $\Delta r_i^n = \left[\begin{array}{cc} \Delta n_i & \Delta e_i \end{array} \right]^T$ and $\Delta\theta_i$ are the translation and rotation parameters from the relative trajectory to the i-th candidate trajectory, the subscript "j" represents the point number. The corresponding rotation matrix from b-frame to n-frame also needs to be adjusted to

$$\left(C_b^{n'}\right)_{i,j} = \left(C_n^{n'}\right)_i \left(C_b^n\right)_j \tag{19}$$

where

$$\left(C_n^{n'}\right)_i = \left[\begin{array}{ccc} \cos\left(\Delta\theta_i\right) & -\sin\left(\Delta\theta_i\right) & 0 \\ \sin\left(\Delta\theta_i\right) & \cos\left(\Delta\theta_i\right) & 0 \\ 0 & 0 & 1 \end{array} \right] \tag{20}$$

The magnetic field map is composed of evenly distributed reference points and MFF at each point (RP), due to the coordinates of a candidate trajectory not coinciding with the RPs. A bilinear interpolation method is used to obtain a reference MFF with higher resolution. As Fig. 4 shows, given the coordinates of an observation point (n, e), the corresponding reference MFF can be approximated using the coordinates of the four closest RPs. A linear interpolation along the north and east

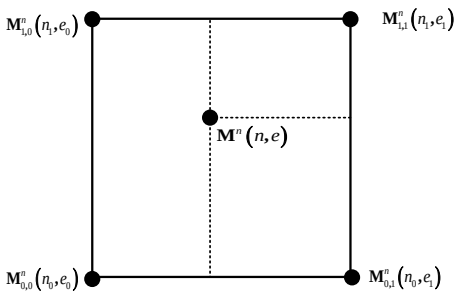

Fig. 4. The reference MFF from bilinear interpolation at position of (n, e).

then yields [24]

$$M^n \approx \alpha_1 M^n_{0,1} + \alpha_2 M^n_{0,0} + \alpha_3 M^n_{1,1} + \alpha_4 M^n_{1,0} \tag{21}$$

$$\begin{aligned} \alpha_1 &= \frac{(n_1-n)(e-e_0)}{(n_1-n_0)(e_1-e_0)}, \alpha_2 = \frac{(n_1-n)(e_1-e)}{(n_1-n_0)(e_1-e_0)} \\ \alpha_3 &= \frac{(n-n_0)(e-e_0)}{(n_1-n_0)(e_1-e_0)}, \alpha_4 = \frac{(n-n_0)(e_1-e)}{(n_1-n_0)(e_1-e_0)} \end{aligned} \tag{22}$$

Then, the reference MFF corresponding to the i-th candidate trajectory can be expressed as:

$$M^n_i = \left[\begin{array}{ccc} \left(M^n_{i,1}\right)^T & \cdots & \left(M^n_{i,j}\right)^T \end{array} \right]^T \tag{23}$$

and the reference MFF in the b-frame can be expressed as:

$$M^b_i = \left[\begin{array}{ccc} \left(C^{n'}_b\right)^T_{i,1} M^n_{i,1} & \cdots & \left(C^{n'}_b\right)^T_{i,j} M^n_{i,j} \end{array} \right]^T \tag{24}$$

Therefore, the i-th reference MFP is:

$$rMFP_i = \left\{ \begin{array}{ccc} r^{n'}_{i,1} & \left(C^{n'}_b\right)_{i,1} & M^b_{i,1} \\ & \cdots & \\ r^{n'}_{i,k} & \left(C^{n'}_b\right)_{i,k} & M^b_{i,k} \end{array} \right\} \tag{25}$$

C. Determination of User's Current Location

As described above, the differential MFP in the b-frame can eliminate the magnetometer bias. However, the noise of the magnetometer is relatively intense, and the selection of the reference value for constructing the differential MFP affects its accuracy. This solution performs de-averaging processing on the observed MFP and the reference MFP, respectively.

Subsequently, the DTW algorithm is used to calculate the similarities between the observed MFP and the reference MFP to determine which candidate reference MFP corresponds to the trajectory of the user's most likely motion. DTW compresses or stretches the reference axis of the two sequences to be matched so that two sequences with different lengths have better matching results [13]. This will help solve the problem of inaccurate estimation of pedestrian step length by the PDR algorithm.

In addition, the results of MFM are used to correct the estimated position of INS-based PDR, which helps improve the estimation accuracy of the relative trajectory (e.g., the scale of step length), and provides a more accurate location search area for the magnetic matching method. The position observation equation in the n-frame is given by:

$$\delta z_r = \hat{r}^n_{INS} - \tilde{r}^n_{MFM} = \delta r^n + n_r \tag{26}$$

where $\hat{r}^n_{INS}$ represents the estimated position by INS mechanization, $\tilde{r}^n_{MFM}$ represents the output of magnetic matching method, and n_r represents the white noise of the position measurement.

VI. Tests and Results

Field tests are conducted in a real indoor office environment with dimensions of approximately 94 m × 22 m, and the indoor building structure is shown in Fig. 5. Four phones (i.e., HUAWEI Mate 20, SAMSUNG S6, Xiaomi 8, and Google Pixel 2) are used for collecting data.

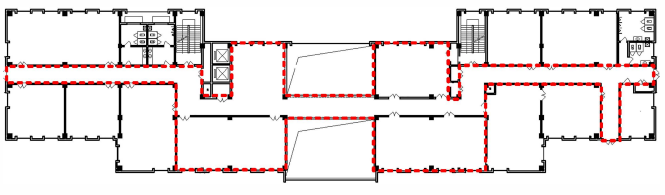

Fig. 5. Floor plan. The test area is the part inside the red box.

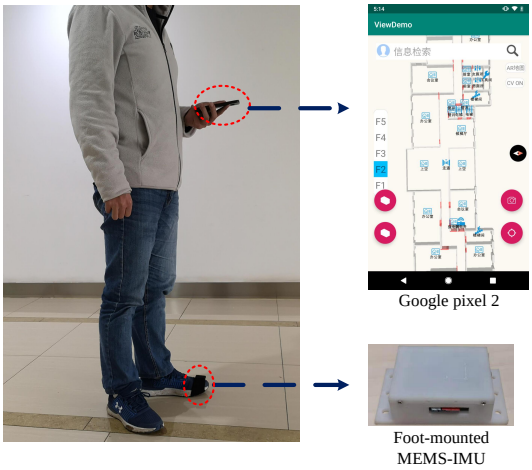

Fig. 6. The structure of P-POS.

We use the P-POS to determine position and attitude of the smartphone to generate the magnetic field map and evaluate the positioning performance of the proposed MFM method. The P-POS consists of a foot-mounted MEMS-IMU and a handheld smartphone, as shown in Fig. 6. Bluetooth communication technology is used to synchronize the system time between the foot-mounted MEMS-IMU and the smartphone. The detailed algorithm and the performance parameters of the foot-mounted MEMS-IMU can be found in [25].

A smartphone (Google Pixel2) is used to collect the magnetic field signals to generate the magnetic field map. An ellipsoid fitting method [26] is employed to calibrate and subtract the magnetometer bias to accurately obtain the indoor magnetic field signals. The magnetic field map consists of uniformly distributed grids, and the grid size is 0.3 m. The magnetic field map of the test area in different directions (i.e., north, east, and vertical) are shown in Fig. 7. The unit is milligauss, denoted as mG.

A total of eight tests are employed for evaluating the positioning performance of the propose MFM algorithm: tests 1 and 2 for HUAWEI Mate 20, tests 3 and 4 for SAMSUNG S6, tests 5 and 6 for Xiaomi 8, and tests 7 and 8 for Google Pixel 2. Due to each test being performed individually, the trajectories of any two tests are slightly different. During the data collection process, the misalignment angle between the tester's walking direction and the smartphone heading should be small. In addition, because the magnetic field feature does not have the ability to uniquely distinguish global position, the initial position is usually given by other methods (such as WiFi or Bluetooth). The initial position is manually given here, the position error is less than 10 m, and the initial heading is

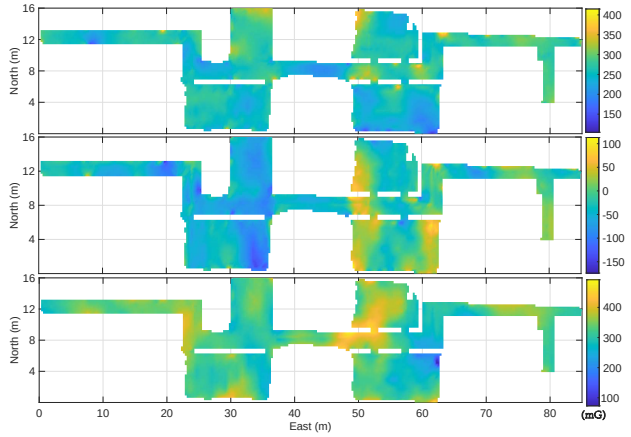

Fig. 7. The magnetic field map of the test area. The upper, middle, and lower graph represent the magnetic field map in the north, east, and vertical direction, respectively.

given by the magnetic field matching algorithm.

A. Positioning Performance Analysis

The positioning performance analysis of three algorithm configurations are used for verifying the feasibility and effectiveness of the proposed MFM method. The three algorithm configurations include: a) the PDR method described in section IV. b) The MFM based on the relative trajectory generated by the PDR. c) On the basis of MFM, the positioning result of MFM is used to control the cumulative error of PDR, referred to as MFM/PDR.

The test trajectories are composed of straight lines and irregular curves to illustrate that the proposed MFM method adapts to the scene of the user's arbitrary walking track. Fig. 8 shows the trajectories of the reference, PDR, MFM and MFM/PDR of eight tests where the red, blue, green and yellow lines represent the reference, PDR, MFM and MFM/PDR trajectory, respectively. The trajectories of PDR exhibit different direction and distance errors due to sensor errors (i.e., the bias of gyroscope) and step-length estimation model errors. The trajectories of MFM and MFM/PDR have a high degree of overlap with the reference trajectory for their stable positioning performance.

Fig. 9 shows the cumulative distribution function (CDF) of PDR, MFM, and MFM/PDR of eight tests. The root mean square (RMS), 68%, and 95% of the position error of the above method are summarized in Table I. The average value of position error are 7.45, 7.97, and 10.85 m for PDR, 1.32, 1.35, and 2.06 m for MFM, and 0.77, 0.77, and 1.42 m for MFM/PDR. Although the relative trajectory generated by PDR have obvious errors in the heading and scale, they can still effectively assist in the implementation of the magnetic field matching positioning algorithm in the b-frame. This mainly because these errors can be tolerated due to the slight changes in magnetic field feature in most indoor areas. At the moment, we find that the position error of MFM/PDR is 0.55 m smaller than that of MFM, and a 41.6% improvement in positioning performance is obtained. Because the output of MFM is used to control the position error of PDR in the MFM/PDR method, the error of sensor and the step length estimation model can be accurately estimated, and the accuracy of the relative trajectory can be continuously improved.

TABLE I
RMS, 68%, AND 95% OF THE POSITION ERRORS OF PDR, MFM AND MFM/PDR

Test	PDR (m)			MFM (m)			MFM/PDR (m)		
	RMS	68%	95%	RMS	68%	95%	RMS	68%	95%
1	9.84	10.57	14.43	1.35	1.40	2.11	0.84	0.82	1.43
2	6.71	7.42	8.66	1.53	1.41	2.17	0.76	0.73	1.32
3	8.13	8.63	12.22	1.19	1.23	1.83	0.71	0.68	1.36
4	7.24	7.46	11.26	1.09	1.14	1.64	0.66	0.72	1.12
5	6.17	6.58	9.60	1.50	1.67	2.33	0.85	0.80	1.62
6	6.73	6.47	11.03	1.42	1.37	2.39	0.84	0.89	1.59
7	6.62	7.49	9.14	1.10	1.17	1.65	0.68	0.73	1.22
8	8.17	9.16	10.49	1.36	1.38	2.36	0.87	0.78	1.72
Mean	7.45	7.97	10.85	1.32	1.35	2.06	0.77	0.77	1.42

B. Comparison of the different DMFFs

We analyze the positioning performance of the different DMFFs in the n-frame. The DMFFs include: 1) vertical component (N1) [18], 2) horizontal and vertical components (N2) [10], and 3) north, east, and vertical components (N3). Additionally, the calibrated MFFs in the n-frame are provided as a comparison, denoted as N0.

Fig. 10 shows the CDF of N0, N1, N2 and N3. The RMS, 68%, and 95% of the position error of the different MFF sequences are summarized in Table II. The average value of position errors are 0.86, 0.83, and 1.58 m for N0; 1.77, 1.47, and 3.65 m for N1; 2.59, 2.18, and 5.34 m for N2,and 3.20, 2.65, and 6.43 m for N3. Because the turning movements and slight fluctuations in attitude are inevitable for almost all users, there are obvious differences in MFM positioning performance when using N1, N2, and N3. The assumption that the attitude of the smartphone remains unchanged or fluctuates slightly cannot be meet because the tester holds the smartphone to collect sensor data. This causes the fluctuation of the horizontal angle (including the roll and pitch) to be small (by a few degrees) compared to the change of the heading angle. The positioning performance of N2 and N3 is noticeably worse than that of N1. In addition, the positioning error of test 7-8 is several times larger than that of test 1-6, as even with small fluctuations in the attitude of the smartphone, a large residual magnetometer bias still causes obvious damage.

The proposed method can achieve positioning performance equivalent to or better than calibrated MFFs of 0.83 m (RMS)due to the working current producing a weak electromagnetic effect in the positioning phase, which causes a change in the magnetometer bias. Compared with the calibrated MFFs, the differential MFP in the b-frame can greatly reduce the influence of these errors.

VII. DISCUSSION

As described in section VI, the positioning error of the proposed method fluctuates from 0.66 to 0.87 m in the 8

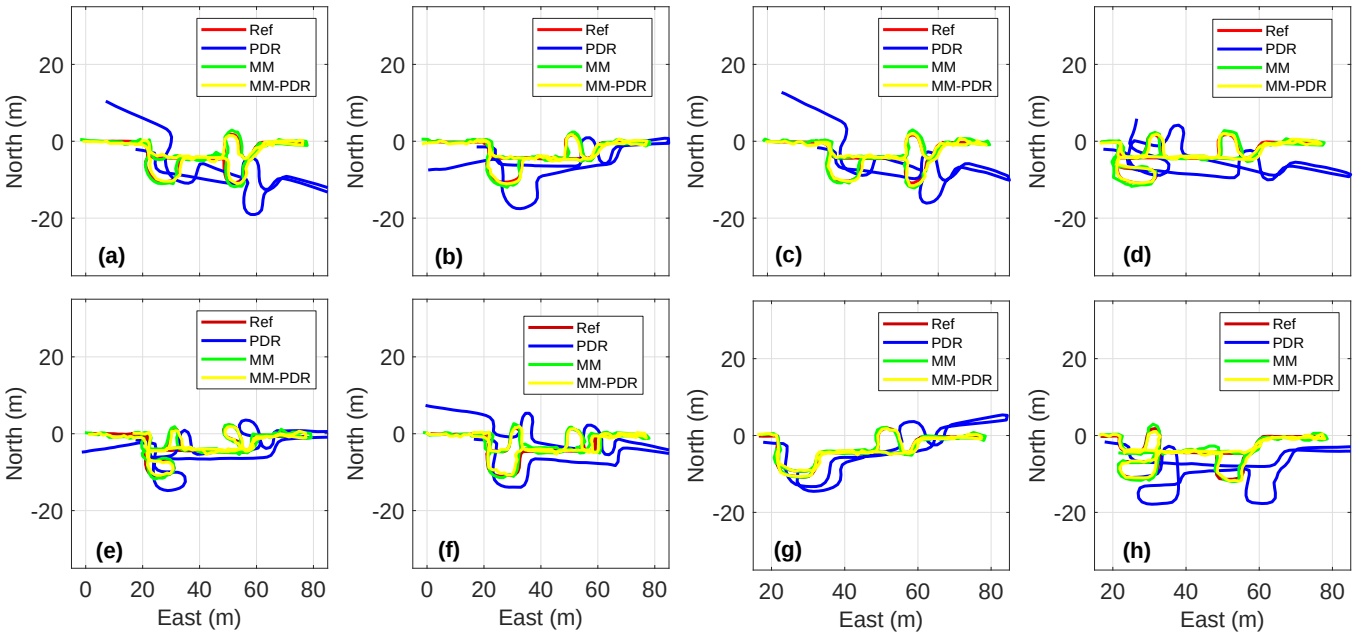

Fig. 8. Trajectories of the reference, PDR, MFM, and MFM/PDR of eight tests. (a)-(h) corresponds to test 1-8. And the red, blue, green and yellow lines represent the reference, PDR, MFM and MFM/PDR trajectory, respectively.

TABLE II
THE RMS, 68%, AND 95% OF THE POSITION ERRORS OF FOUR DMFFS

Test	N0 (m)			N1 (m)			N2 (m)			N3 (m)		
	RMS	68%	95%	RMS	68%	95%	RMS	68%	95%	RMS	68%	95%
1	1.01	0.98	1.85	1.28	1.27	2.22	1.08	1.05	2.06	1.10	1.10	2.06
2	1.00	0.88	1.86	0.99	1.02	1.85	1.03	0.99	2.07	1.11	1.09	1.90
3	0.79	0.80	1.37	1.15	1.13	2.25	2.46	1.53	5.41	1.91	1.29	4.84
4	0.72	0.70	1.23	1.11	1.01	1.77	2.79	1.69	6.11	3.00	1.63	7.05
5	0.87	0.86	1.55	1.10	1.03	2.19	2.93	1.79	6.45	3.89	2.84	8.23
6	0.94	0.97	1.63	1.25	1.17	2.14	2.43	1.73	5.15	4.37	2.61	9.03
7	0.71	0.70	1.43	3.51	2.18	8.75	3.87	4.11	7.57	5.06	4.89	9.71
8	0.87	0.75	1.75	3.77	2.95	8.01	4.12	4.54	7.89	5.21	5.72	8.60
Mean	0.86	0.83	1.58	1.77	1.47	3.65	2.59	2.18	5.34	3.20	2.65	6.43

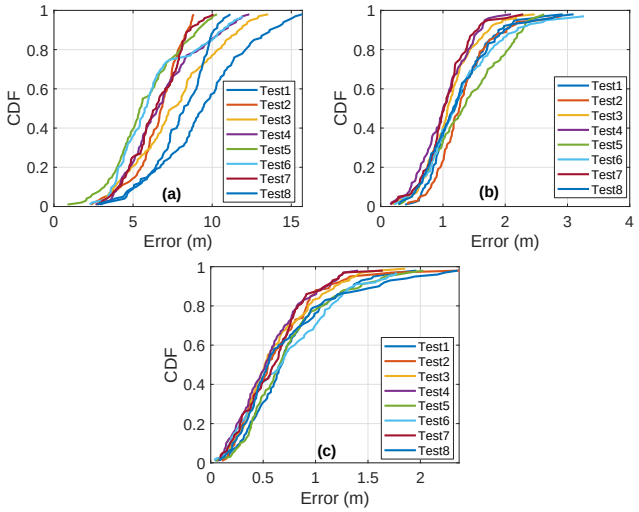

Fig. 9. The CDF of PDR, MFM, and MFM/PDR of eight tests. (a) PDR, (b) MFM, (c) MFM/PDR.

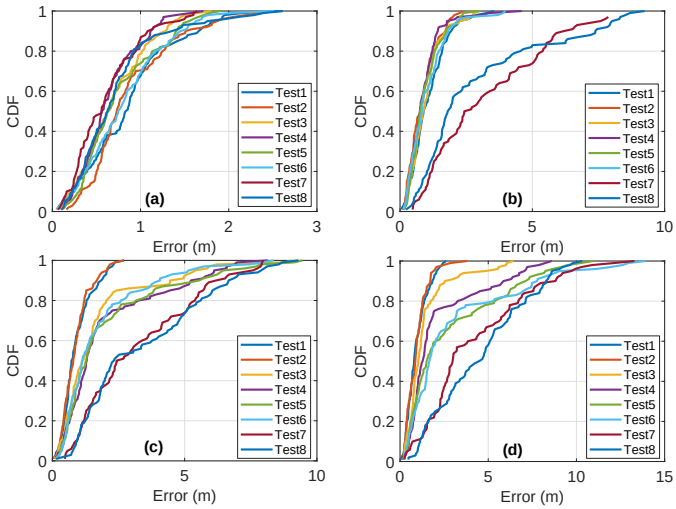

Fig. 10. The CDF of N0, N1, N2 and N3. (a) N0, (b) N1, (c) N2, (d) N3.

tests based on 4 smartphones, achieving an average position error of 0.77 m (RMS). In the absence of magnetometer bias calibration, the position performance of the differential magnetic field profile can reach or even outperform the calibrated MFFs. Thus, the proposed MFM algorithm has stable positioning performance and is not affected by the magnetometer bias, and there is no significant difference in positioning performance for different smartphone hardware. The reasons can be summarized as follows: 1) the accuracy of the relative trajectory and attitude of the differential MFP are sufficient to cancel the magnetometer bias. Thus, only the stability of MFFs over a short period (e.g., 15 s) will have a significant impact on the positioning performance. The electromagnetic phenomenon formed by the current change of the device will only cause short-term impact. 2) The strong correlation information between the three-dimensional MFFs and the geographic spatial coordinates is established, which has better position discrimination. 3) The precise predicted position can be used to control the search area of the MFM, thereby greatly reducing the probability of a mismatch.

However, the positioning performance of the MFM/PDR method is very dependent on the relative integrity of the PDR. The problem of frequent and unpredictable change in the misalignment angle between the orientation of the mobile phone and the walking direction of the user will continue to seriously damage the stability of the MFM/PDR.

VIII. Conclusion

In this study, we present a magnetic field matching method insensitive to magnetometer bias based on PDR for smartphones positioning in an indoor environment. An INS-based PDR is designed to generate the relative trajectory and the attitude of a smartphone for MFM. The relative trajectory is used to correlate the MFF time sequence for improving the distinguishability and constraining the search region of MFM by predicting position. The attitude is used for projecting the reference MFP from n-frame to b-frame, to perform the MFM in the b-frame and eliminating the influence of the magnetometer bias.

To evaluate the positioning performance of the proposed method, we conduct eight experiments using four smartphones in the same building. Although the proposed MFM algorithm does not perform bias compensation for the magnetometer observations, it can still obtain a stable positioning result and achieve a positioning performance equivalent to that of the calibrated magnetometer observation. The test results show that the positioning error is distributed between 0.66 and 0.87 m, reaching an average positioning performance of 0.77 m (RMS). The experimental results completely verify that the MFM method designed in this study is less affected by the magnetometer bias, and there is no significant difference in positioning performance between different smartphones.

In our future work, we will test the positioning performance of the proposed method in multiple typical smartphone poses, i.e., handheld, calling, swinging in hand, and in pant pockets for adaptation to the user's behavior. In addition, we will attempt to perform a global traversal search in the magnetic field map so that the position and direction can be initialized using only the MFM method, which will be helpful for providing positioning service for users in regions with only magnetic field signals.

References

[1] I. A. Junglas and R. T. Watson, "Location based services", Commun. ACM, vol. 51, issue 3, pp. 65-69, Mar. 2008.

[2] H. Kuusniemi, M. Z. H. Bhuiyan, M. Ström, S. Söderholm, T. Jokitalo, L. Chen, and R. Chen, "Utilizing pulsed pseudolites and high-sensitivity gnss for ubiquitous outdoor/indoor satellite navigation," in Proc. Int. Conf. Indoor Positioning Indoor Navigat. (IPIN), Nov. 2012, pp. 1–7.

[3] A. S. I. Noh, W. J. Lee, and J. Y. Ye, "Comparison of the mechanisms of the Zigbee's indoor localization algorithm," in Proc. 9th ACIS Int. Conf. Softw. Eng., Artif. Intell., Netw., Parallel/Distrib. Comput., Phuket, Thailand, 2008, pp. 13–18.

[4] J. Yan, "Algorithms for indoor positioning systems using ultra-wideband signals," Ph.D. dissertation, Master Sci. Eng., , Chalmers Univ. Technol., Gothenburg, Sweden, 2010.

[5] T. Liu, X. Niu, J. Kuang, S. Cao, L. Zhang and X. Chen, "Doppler shift mitigation in acoustic positioning based on pedestrian dead reckoning for smartphone," IEEE Trans. Instrum. Meas., vol. 70, pp. 1-11, 2021.

[6] A. Bekkali, H. Sanson, and M. Matsumoto, "RFID indoor positioning based on probabilistic RFID map and Kalman filtering," in Proc. 3rd IEEE Int. Conf. Wireless Mobile Comput., Netw. Commun., 2007, pp. 21–28.

[7] Y. Li, Y. Zhuang, H. Lan, P. Zhang, X. Niu, and N. El-Sheimy, "WiFi-aided magnetic matching for indoor navigation with consumer portable devices," Micromachines, vol. 6, no. 5, pp. 747–764, 2015.

[8] J. Kuang, X. Niu, P. Zhang, and X. Chen, "Indoor positioning based on pedestrian dead reckoning and magnetic field matching for smartphones," Sensors, vol. 18, no. 12, pp. 4142, 2018.

[9] J. Kuang, X. Niu, and X. Chen, "Robust pedestrian dead reckoning based on mems-imu for smartphones," Sensors, vol. 18, no. 5, pp. 1391, 2018.

[10] Y. Li, "Integration of MEMS sensors, WiFi, and magnetic features for indoor pedestrian navigation with consumer portable devices," Ph. D. dissertation, Dept. Geomatics Eng., Univ. Calgary, Calgary, AB, Canada, 2016.

[11] L. Hou, Y. Li, Y. Zhuang, B. Zhou, G.-J. Tsai, Y. Luo, and N. El-Sheimy, "Orientation-aided stochastic magnetic matching for indoor localization," IEEE Sens. J., vol. 20, no. 2, pp. 1003–1010, Jan 2020.

[12] E. Le Grand and S. Thrun, "3-axis magnetic field mapping and fusion for indoor localization," in Proc. IEEE Int. Conf. Multisensor Fusion Integr. Intell. Syst. (MFI), Sep. 2012, pp. 358–364.

[13] K. P. Subbu, B. Gozick, and R. Dantu, "LocateMe: Magnetic-fieldsbased indoor localization using smartphones," ACM Trans. Intell. Syst. Technol., vol. 4, no. 4, 2013, Art. no. 73.

[14] T. Ozyagcilar, "Calibrating an ecompass in the presence of hard and soft-iron interference," Freescale Semiconductor Ltd., 2012.

[15] Y. Wu, D. Zou, P. Liu, and W. Yu, "Dynamic magnetometer calibration and alignment to inertial sensors by Kalman filtering," IEEE Trans. Control Syst. Technol., vol. 26, no. 2, pp. 716–723, Mar. 2018.

[16] A. Wahdan, J. Georgy, and A. Noureldin, "Three-dimensional magnetometer calibration with small space coverage for pedestrians," IEEE Sens. J., vol. 15, no. 1, pp. 598–609, Jan. 2015.

[17] J. Liu, R. Chen, L. Pei, R. Guinness, and H. Kuusniemi, "A hybrid smartphone indoor positioning solution for mobile LBS," Sensors, vol. 12, no. 12, pp. 17208–17233, 2012.

[18] B. Kim and S.-H. Kong, "A novel indoor positioning technique using magnetic fingerprint difference," IEEE Trans. Instrum. Meas., vol. 65, no. 9, pp. 2035–2045, Sep. 2016.

[19] H. Xie, T. Gu, X. Tao, H. Ye, and J. Lv, "Maloc: A practical magnetic fingerprinting approach to indoor localization using smartphones," in Proc. ACM Int. Joint Conf. Pervasive Ubiquitous Comput., 2014, pp. 243–253.

[20] E.-H. Shin, "Estimation techniques for low-cost inertial navigation," Ph.D. dissertation, Dept. Geomatics Eng., Univ. Calgary, Calgary, AB, Canada, 2005.

[21] E. Foxlin, "Pedestrian tracking with shoe-mounted inertial sensors," IEEE Comput. Graph. Appl., vol. 25, no. 6, pp. 38–46, Nov. 2005.

[22] A. Brajdic and R. Harle, "Walk detection and step counting on unconstrained smartphones," in Proc. ACM Int. Joint Conf. Pervasive Ubiquitous Comput., 2013, pp. 225–234.

[23] P. Davidson and J. Takala, "Algorithm for pedestrian navigation combining IMU measurements and gait models," J. Gyroscopy Navig., vol. 4, no. 2, pp. 79–84, 2013.
[24] S. Kohlbrecher, J. Meyer, O. von Stryk, and U. Klingauf, "A flexible and scalable SLAM system with full 3D motion estimation," in Proc. IEEE Int. Symp. Safety, Secur. Rescue Robot. (SSRR), Nov. 2011, pp. 155–160.
[25] X. Niu, T. Liu, J. Kuang and Y. Li, "A Novel Position and Orientation System for Pedestrian Indoor Mobile Mapping System," IEEE Sens. J., vol. 21, no. 2, pp. 2104-2114, 15 Jan., 2021.
[26] S. A. H. Tabatabaei, A. Gluhak, and R. Tafazolli, "A fast calibration method for triaxial magnetometers," IEEE Trans. Instrum. Meas., vol. 62, no. 11, pp. 2929–2937, Nov. 2013.

Jian Kuang received the B.Eng. degree and Ph.D. degree in Geodesy and Survey Engineering from Wuhan University, Wuhan, China, in 2013 and 2019, respectively. He is currently a Postdoctoral Fellow with the GNSS Research Center in Wuhan University, Wuhan, China. His research interests focus on inertial navigation, pedestrian navigation and indoor positioning.

Taiyu Li received the B.Eng. degree in Geodesy and Survey Engineering from China University of Mining and Technology, Xuzhou, China, in 2019. He is currently a Master student in the GNSS Research Center, Wuhan University, Wuhan, China. His research interests focus on pedestrian navigationand indoor positioning.

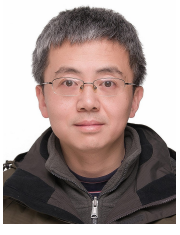

Xiaoji Niu received the B.Eng. degree (with honors) in Mechanical and Electrical Engineering and the Ph.D. from Tsinghua University, Beijing, China. He was a Post-Doctoral Fellow with the Mobile MultiSensor Systems (MFMSS) Research Group, Department of Geomatics Engineering, and University of Calgary. He was a Senior Scientist with SiRF Technology, Inc. At present, he is a Professor of the GNSS Research Center and the Collaborative Innovation Center of Geospatial Technology in Wuhan University, Wuhan, China. His research interests focus on INS, GNSS/INS integration for land vehicle navigation and pedestrian navigation.